# CHAPTER 5

# RESULTS

In chapter 4, all the ingredients to calculate the antiproton to proton flux ratio are given. In this chapter, the calculated antiproton to proton flux ratio in time averaged and time dependent analysis is shown.

## 5.1. Time Averaged Result

In August 2016, the AMS-02 collaboration published the time-averaged antiproton to proton flux ratio up to 450 GV with four years data (taken from May 2011 to May 2015). In Feb 2021, the AMS-02 collaboration published the flux ratio up to 525 GV with six and half years data. Nowadays, the data has been taken continuously up to May 2021, and this analysis is based on the latest ten years data. With more data, the antiproton to proton flux ratio can be updated with higher statistics and improved accuracy.

Since the antiproton to proton flux ratio is determined in three different ranges, the time-averaged antiproton to proton flux ratio is given in figure 5.1 with the overlapping range. The results in the overlapping range are consistent with each other. In figure 5.2, the final antiproton to proton flux ratio in this analysis is shown.

In the highest rigidity range, the antiproton to proton ratio shows a relatively flat trend. No obvious falling trend is observed as the positron to electron flux ratio shown in the latest paper from AMS-02 collaboration [107] . To observe the behavior in a higher rigidity range, more data is required and better charge confusion separation is needed.

To check the consistency between the result in this analysis and in AMS-02 published result in Physics Report [107] , the same data period is used. In figure 5.3, the antiproton to proton flux ratios in this analysis based on six and half years data is shown. Compared with the result in Physics Report based on the same data period, the result in this analysis, as an independent analysis, matches well within the error bars.

The total error breakdown is shown in 5.4. In the high rigidity range, the error is mainly dominated by systematic error due to the dominant background of charge confused protons and limited

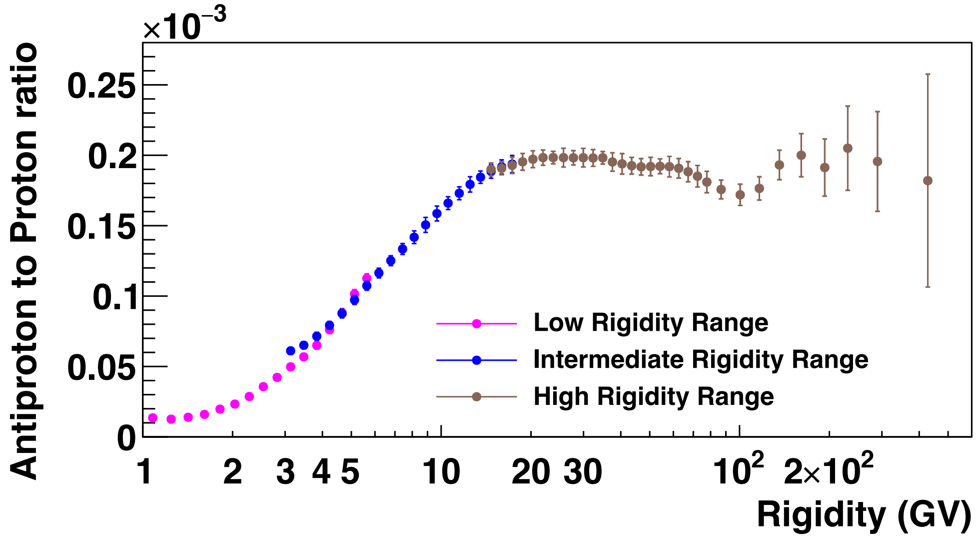


Figure 5.1: The time-averaged antiproton to proton flux ratios in three rigidity ranges is shown. In the overlapping ranges, the results from different template fit methods are consistent with each other. The error bars are total errors calculated from the quadratic sum of statistical and systematic errors.

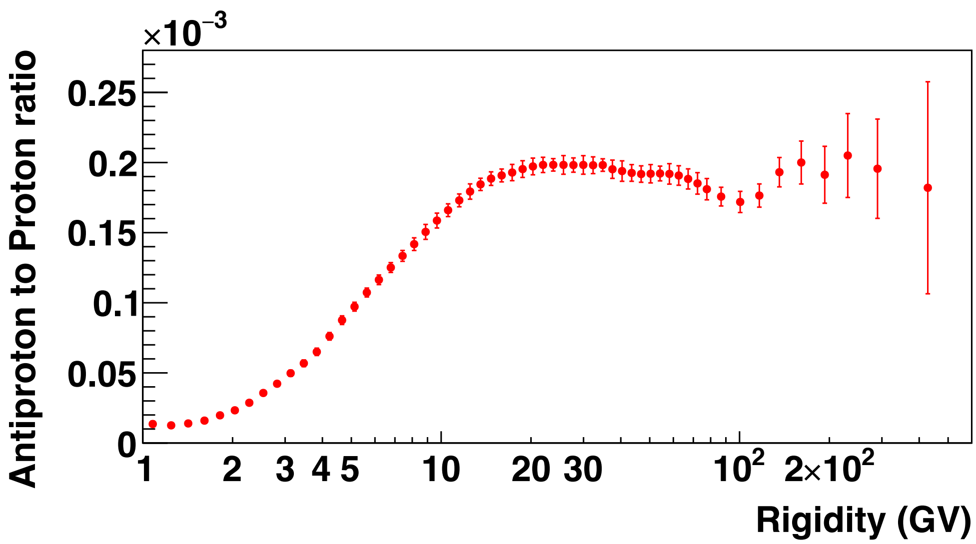


Figure 5.2: The final result of the time-averaged antiproton to proton flux ratio with the data taken from May 2011 to May 2021 in this analysis. The error bar is the total error calculated from the quadratic sum of statistical and systematic error.

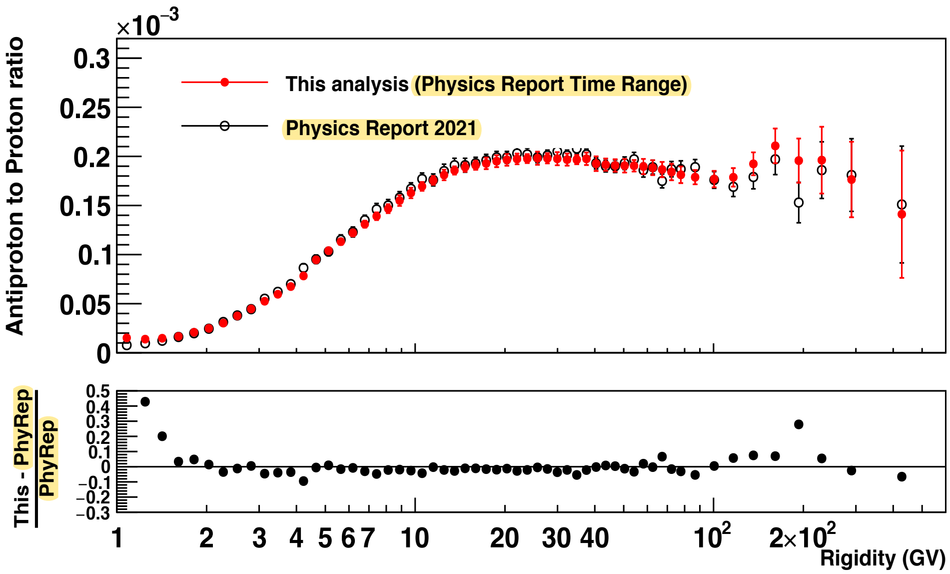


Figure 5.3: Comparison between the antiproton to proton flux ratio in this analysis and in Physics Report [107] , both of the two flux ratios use six and half years of data. The two results match with each other within the error bars.

separation power. In the intermediate range, the error is dominated by systematic error due to the effective acceptance. In the lowest rigidity range, namely below 2 GV, the contributions from statistical and systematic error are at a similar level, which is much improved from the previous antiproton publication with four years data collected.

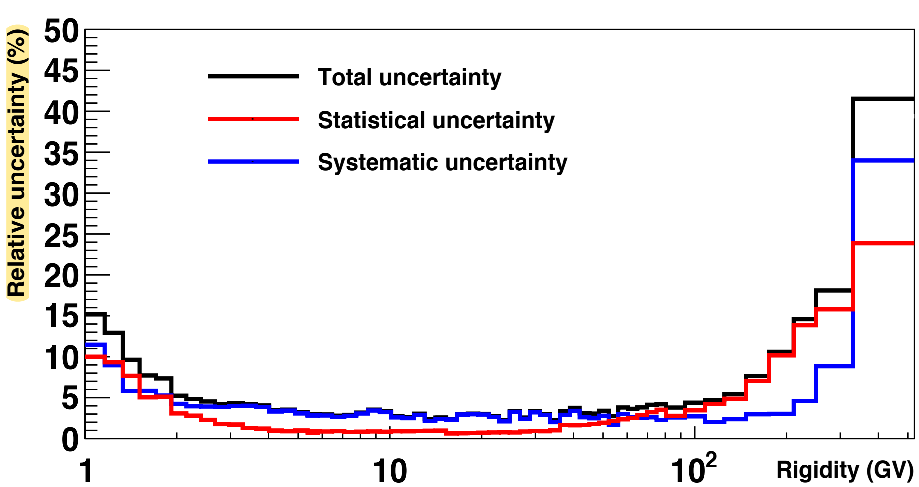


Figure 5.4: The uncertainty breakdown of the time-averaged antiproton to proton flux ratio in this analysis. In the highest rigidity bin, the systematic uncertainty is dominated due to the charge confusion protons. In the low rigidity range, the statistical uncertainty and systematic uncertainty make similar contributions.

## 5.2. Time Dependent Result

Apart from the time-averaged antiproton to proton flux ratio, the time-dependent antiproton to proton flux ratio can also be calculated with the same strategy. For the time-dependent analysis, the antiproton to proton flux ratio is determined in six Bartels Rotations. In total, 14 time-dependent antiproton to proton flux ratios are obtained from 1.16 GV to 18 GV. The time-dependent antiproton to proton flux ratio is given in 5.5. In this figure, the variation caused by solar modulation is clearly shown.

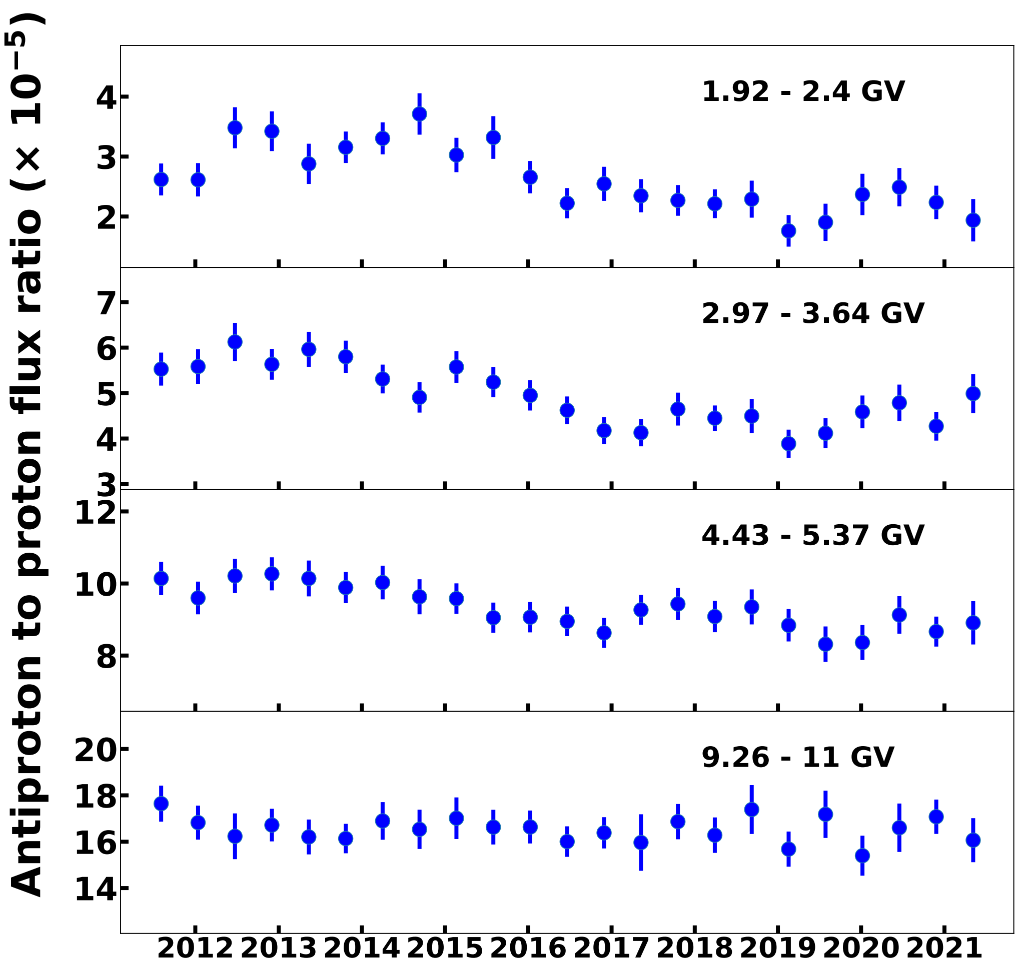


Figure 5.5: Time-dependent antiproton to proton flux ratios for four of the 14 rigidity bins. The error bars in this figure are total errors, including statistical errors and systematic errors. Distinct time variation structures are visible in these ratios.

One important observation is that with the rigidity going up, the solar modulation effect is weaker. In the first rigidity bin in this figure, the flux ratio changes by a factor 2 between its minimum and maximum, while in the last one, the fluctuation only changes around 20%. Above 15 GV, the modulation effect is ignorable, and the fluctuation is mainly dominated by noise.

In general, the antiproton to proton flux ratio shows a rising trend up to around 2014, then gradually going down up to the beginning of 2017. After 2017, the flux ratio is relatively flat but slowly rising.

Apart from the long-time trend, there are few fine time structures like around the beginning of 2013, the ratio fell quickly and then recovered soon. Those fine time structures need to be studied in detail with fine time bins.

For illustration, the total error breakdown in an example rigidity bin of 1.92 - 2.4 GV is shown in 5.6. Because of the limited statistics in six Bartels Rotations, the statistical error is dominant in time-dependent results.

In 5.7, the statistical error contributions in total error in 1.92- 2.4 GV is shown, and the statistical error shows a relatively rising trend from 60% to almost 80%.

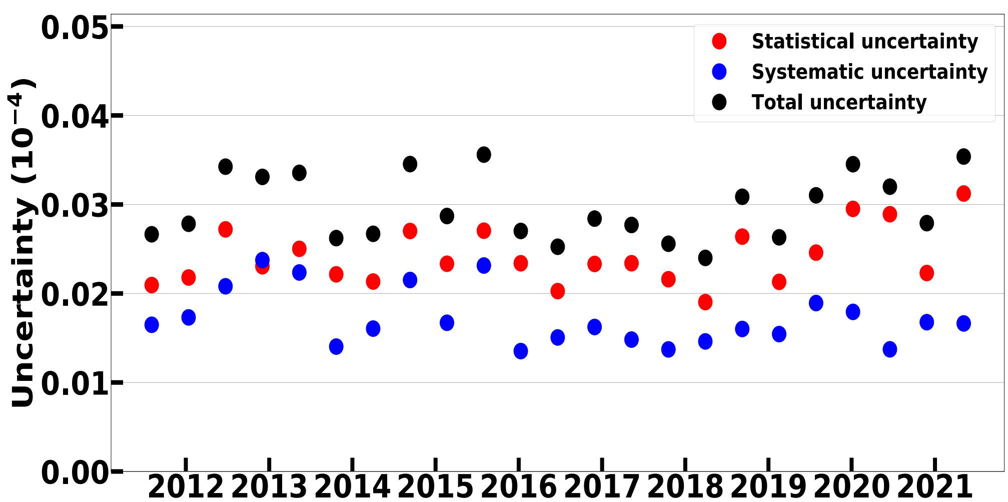


Figure 5.6: Breakdown of the total uncertainty of the antiproton to proton flux ratio into a statistical and systematical part in 1.92 to 2.4 GV.

In figure 5.8, the time-averaged antiproton to proton flux ratio and the 23 time-dependent antiproton to proton flux ratios are shown. The time-dependent antiproton to proton flux ratios have some time-dependent variations but mainly fluctuate around the time-averaged antiproton to proton flux ratio.

To compare further between the time-averaged and dependent antiproton to proton flux ratio, the

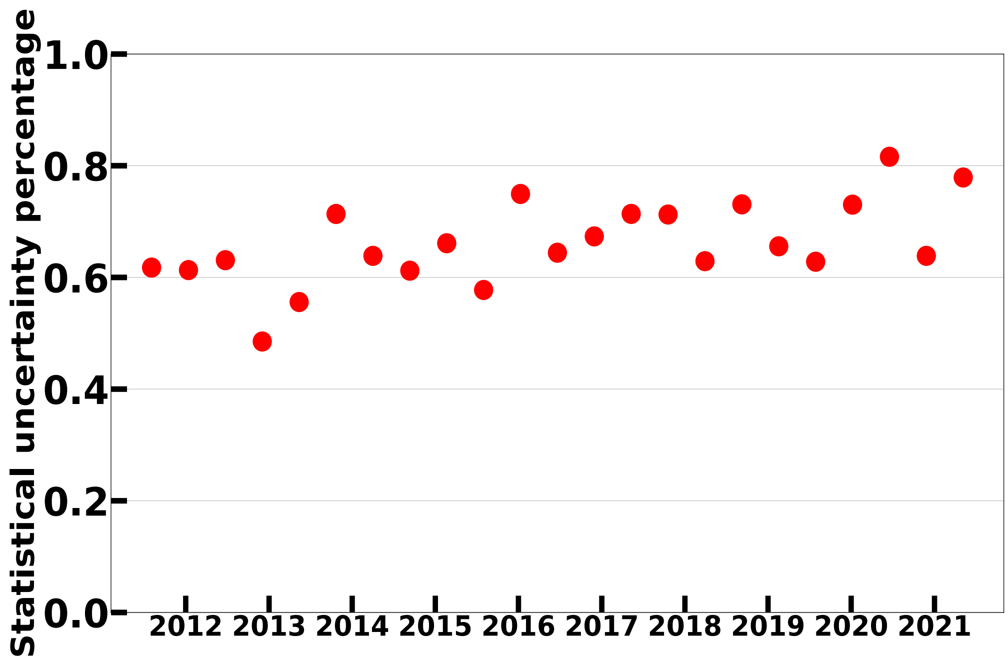


Figure 5.7: Percentage of statistical uncertainty in total uncertainty of the antiproton to proton flux ratio in 1.92 - 2.4 GV.

merging of the time-dependent numbers is done. In each rigidity bin, the 23 time-dependent antiproton numbers and proton numbers are merged respectively. Then the merged antiproton to proton flux ratios is constructed.

In figure 5.9, the time-averaged antiproton to proton flux ratio and the merged antiproton to proton flux ratio are shown. From this comparison, the merged time-dependent antiproton to proton flux ratio match well with the time-averaged antiproton to proton flux ratio, while in the first few bins, the merged antiproton to proton flux ratio deviates a little due to the low statistics.

Since the solar variation affects all kinds of cosmic rays, the obtained time-dependent antiproton to proton flux ratio can be compared with other results. In figure 5.10, the antiproton to proton flux ratio in this analysis is shown together with the electron to positron flux ratio. The electron to positron flux ratio is taken from [103] , and the result is consistent with previous AMS-02 publication in [48] but with a data extension. The electron to positron flux ratio is presented in its ECAL energy bins. To compare in the exact same rigidity bin as used for antiproton to proton flux ratio, the electron and positron fluxes are fitted with a power-law modulated according to the force-field approximation, then integrated the electron and positron fluxes over the rigidity bin used for the antiproton to proton flux ratio, at last, the electron to positron flux ratio in antiproton to proton flux ratio bins can be obtained. Due to the charge sign difference, the two flux ratios are shown in negative charge particles over positive charge particles. The normalization of electron to positron flux ratio is based on the first two years data to make sure the mean of electron to positron flux

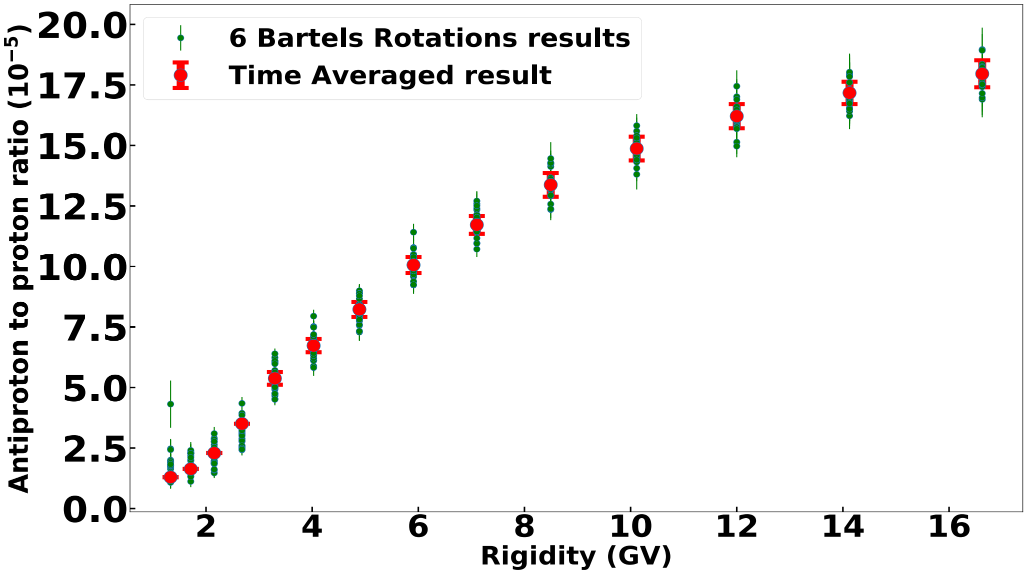


Figure 5.8: time-averaged antiproton to proton flux ratio (red) and 23 time-dependent antiproton to proton flux ratios in six Bartels rotations (green). The time-dependent results are changed around the time-averaged result.

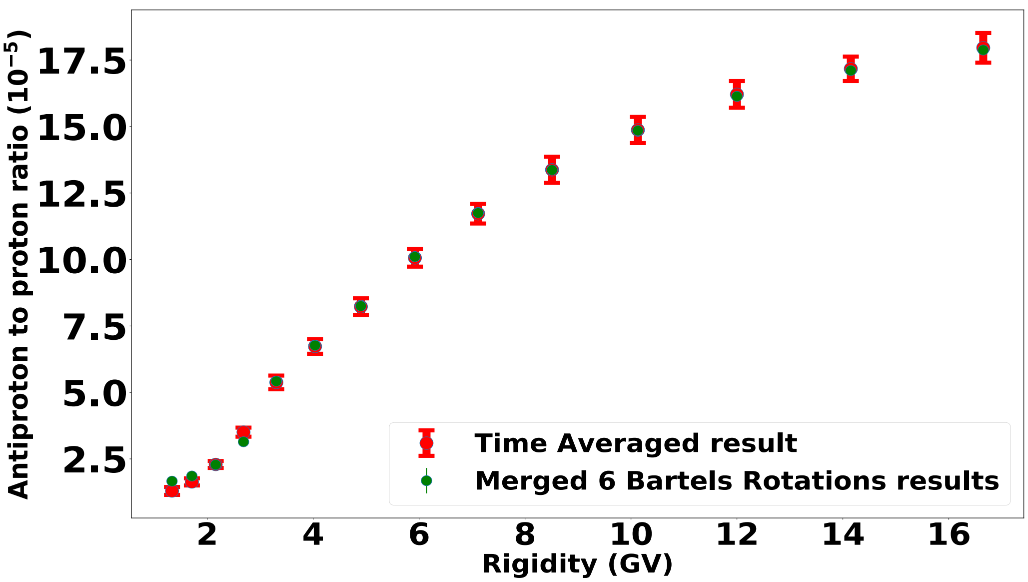


Figure 5.9: Time-averaged antiproton to proton flux ratio (red) and merged time-dependent antiproton to proton flux ratios in six Bartels rotations (green). The merged time-dependent result matches well with the time-averaged result.

ratio is the same as the mean of the antiproton to proton flux ratio.

By comparing the antiproton to proton flux ratio and electron to positron flux ratio, the first observation is the time variation effects in both flux ratios are decreasing with rigidity going up and this observation is expected.

The second observation is the time variation trend of the antiproton to proton flux ratio is different from the electron to positron flux ratio in the low rigidity range. For example, below 3 GV, both ratios go up first and then drop down to the minimum, at last gradually rebound. While the antiproton to proton flux ratio seems to have a delay than the electron to positron flux ratio. This difference gradually gone with the rigidity going up, and the trend of the two ratios become similar in rigidity higher than 6 GV.

For solar modulation modeling, the Local Interstellar Spectra (LIS) are important inputs. The LIS of antiproton and positron are different [108] . Therefore, this could lead to a difference between antiproton to proton flux ratio trend and electron to positron flux ratio trend. Another important difference is the mass difference. Antiproton and proton have much larger mass than electron and positron. This difference has much impact in the lower rigidity range. So, both two reasons could result in different flux ratios in the low rigidity range.

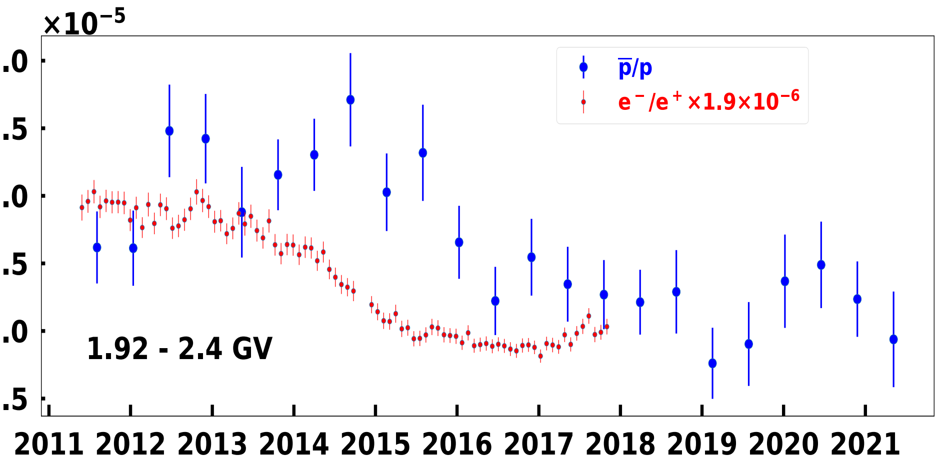
×10⁻⁵
p̄/p
e⁻/e⁺ ×1.9×10⁻⁶
1.92 - 2.4 GV
4.0
3.5
3.0
2.5
2.0
1.5
2011 2012 2013 2014 2015 2016 2017 2018 2019 2020 2021

(a)

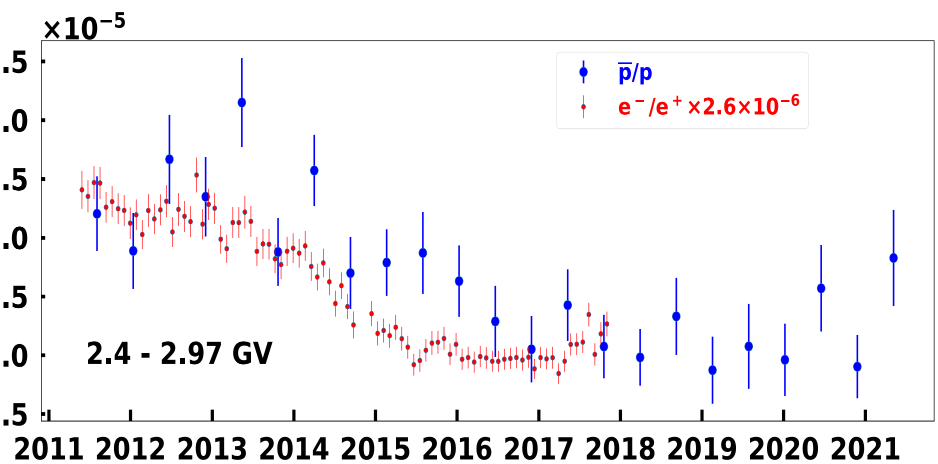
×10⁻⁵
p̄/p
e⁻/e⁺ ×2.6×10⁻⁶
2.4 - 2.97 GV
5.5
5.0
4.5
4.0
3.5
3.0
2.5
2011 2012 2013 2014 2015 2016 2017 2018 2019 2020 2021

(b)

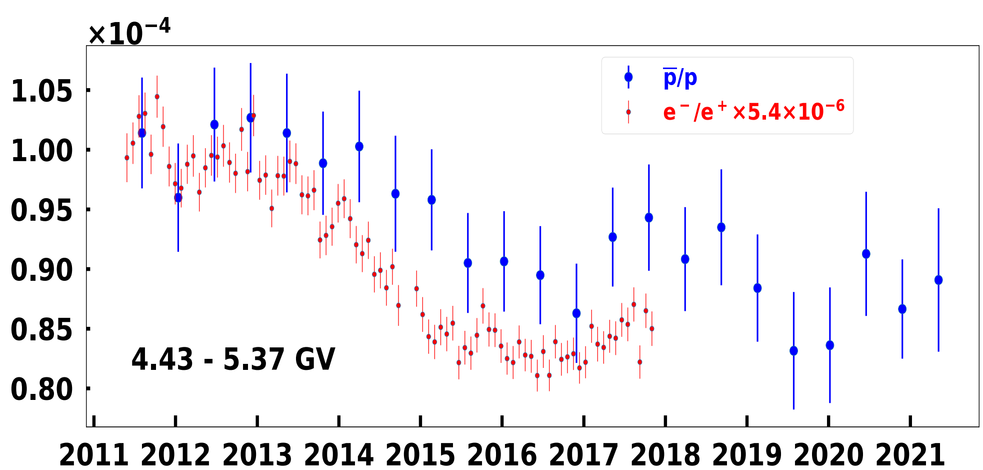
×10⁻⁴
p̄/p
e⁻/e⁺ ×5.4×10⁻⁶
4.43 - 5.37 GV
1.05
1.00
0.95
0.90
0.85
0.80
2011 2012 2013 2014 2015 2016 2017 2018 2019 2020 2021

(c)

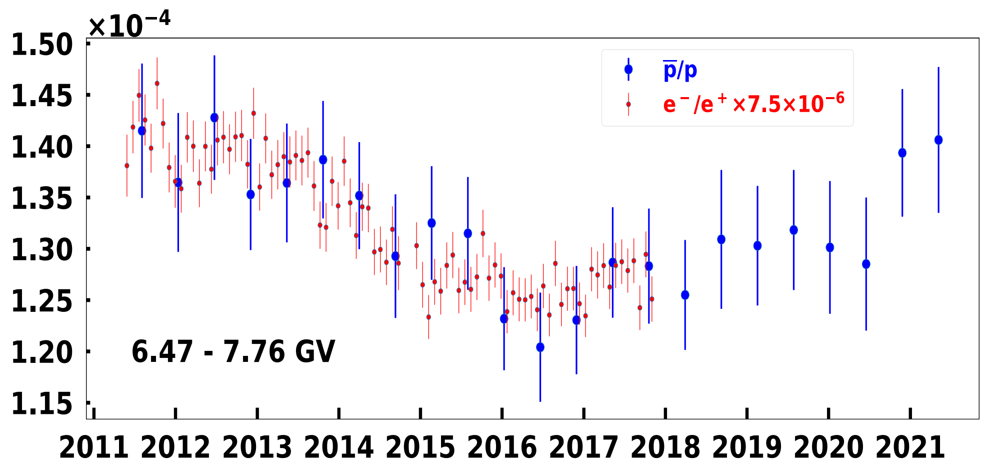


(d)

Figure 5.10: Comparison between antiproton to proton flux ratio (blue) and electron to positron flux ratio (red) in four rigidity bins: a). 1.92-2.4 GV b). 2.4-2.97 GV c). 4.43-5.37 GV d). 6.47-7.76 GV. The error bars are the total errors calculated from the quadratic sum of statistical errors and systematic errors.

# CHAPTER 6

# SUMMARY

In the thesis, the time-averaged antiproton to proton flux ratio is presented up to 525 GV with ten years of AMS-02 cosmic rays data, which is the highest and most accurate measurement up to date. The unprecedented accuracy provides a probe for us to understand the origin of cosmic ray antiprotons. The antiproton to proton flux ratio in the high rigidity range shows a flat trend in previous AMS-02 publication with four years data [1] , instead of a falling trend predicted by secondary production models [26, 27] . This observation doesn't change in this analysis result with the latest ten years data. This analysis is an independent result of the AMS-02 Physics Report result in [107] , which also presents the antiproton to proton flux ratio up to 525 GV.

Except the time-averaged antiproton to proton flux ratio, the time-dependent antiproton to proton flux ratio in every six Bartels Rotations data is presented in this thesis. From 1.16 GV to 18 GV, the time-dependent antiproton to proton flux ratios are given in 14 rigidity bins. The rigidity bins are merged in every two rigidity bins in time-averaged analysis to increase the statistics.

The first observation is that with rigidity going up, the solar modulation effect is weaker. The antiproton to proton flux ratio shows a distinct time structure up to around 15 GV. The data is taken from May 2011 to May 2021, which covers eight years in solar cycle 24 and two years in solar cycle 25. In this period, the behavior of the antiproton to proton flux ratio shows a rising trend first and going down to the minimum, at last gradually going up. This behavior can be used to compare and check with solar modulation models [109, 108] .

The second observation is from the comparison between the antiproton to proton flux ratio and the electron to positron flux ratio. The antiproton to proton flux ratio is different from the electron to positron flux ratio below 3 GV, and this difference gradually gone with rigidity going up. Above 6 GV, this difference almost disappears and the two flux ratios show a similar trend. The different behaviors could be due to the different LIS of antiprotons and positrons in the low rigidity range, therefore they are subject to different modulation results. In addition, the mass difference between antiproton (proton) and positron (electron) also plays important role in the low rigidity range.

AMS-02 will continue to collect data until the lifetime of ISS, which is estimated to be 2030. The improved statistics will reduce the statistical error further in the high rigidity range and give a more precise measurement. For time-dependent analysis, the time variation effect on the antiproton to proton flux ratio has already been shown in ten years period in this work. With the data collected in the future, the time variation effect in the complete 11 years solar cycle can be obtained. On the other hand, the antiproton to proton flux ratio in six Bartels Rotations time resolution shows the time structure in the long time period, the observation of fine time structure requires higher time resolutions. To achieve this, improved analysis method with higher statistics in each time-dependent period allows a stable result in finer time resolution.

After the AMS-02 experiment, a next-generation magnetic spectrometer in space called AMS-100 is in progress [110] , which will be placed on the Lagrange point L2 in around 2039. The AMS-100 can provide 100 $m^2sr$ acceptance and allow a measurement of the antiproton to proton flux ratio up to 10 TV. For the time-dependent analysis, the AMS-100 can continue the study of the solar modulation on the cosmic antiprotons for decades.

# APPENDIX

# Input variables for charge confusion

Except for the four variables shown in section 4.2, the full list of the 12 left input variables used in the training charge confusion estimator is given in this appendix. Nine of them are constructed from the Tracker, two of them are constructed from the TOF, and one of them is constructed from the TRD.

1. **Rigidity Asymmetry and Matching**

   The rigidity is constructed from the Tracker. With the different tracker layers, different rigidity values are obtained. Therefore, the asymmetry and matching variables can be constructed further and used as the inputs of training. Twi variables related to this are used: RigidityAsymmetryL9 and L24L58RigidityMatching. The definitions are given below:

$$\text{RigidityAsymmetryL9} = \frac{\text{RigidityInnerL9} - \text{RigidityInner}}{\text{RigidityInnerL9} + \text{RigidityInner}}$$

$$\text{L24L58RigidityMatching} = \left[\left(\frac{1.0}{\text{RigidityInnerUpper}}\right) - \left(\frac{1.0}{\text{RigidityInnerLower}}\right)\right] \cdot \frac{100\text{R}}{|\text{R}|}$$

   where the RigidityInner and RigidityInnerL9 are the rigidities constructed from the inner tracker layer and the inner tracker layer plus layer 9, RigidityInnerUpper and RigidityInnerLower are constructed from the upper half of the inner tracker layer and the lower half of the inner tracker layer.

   In figure 1, the distributions of the two variables are shown.

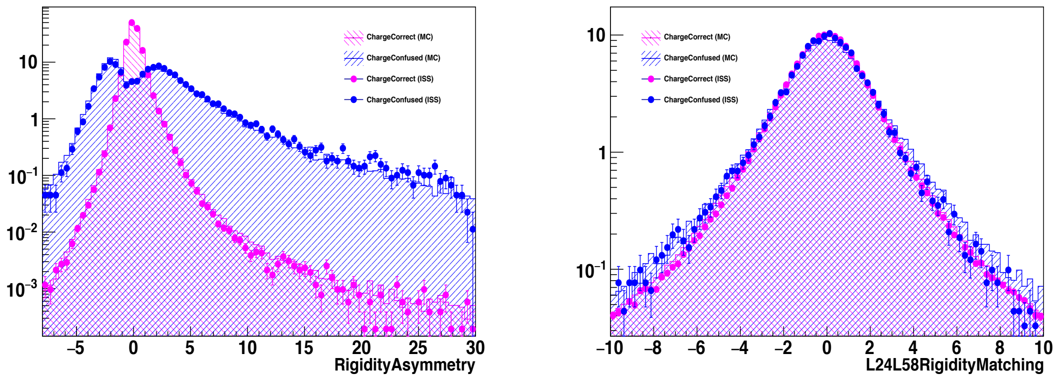


(a) (b)

Figure 1: Distributions of a). RigidityAsymmetry b). L24L58RigidityMatching in example rigidity bin of 330 to 525 GV. Histograms (magenta: charge correct; blue: charge confused) are taken from MC and points (magenta: charge correct; blue: charge confused) are from data.

2. **Tracker Fit Chi2**

The tracker track fit quality provides important information for charge confusion. Due to the interaction, the poorer fit quality, the more likely to be charge confused event. Therefore, the fit Chi2 could be used as the input for training. In total, four variables related to Chi2 are used: Log10Chi2TrackerX and Log10Chi2TrackerY are the tracker track fit Chi2 in logarithmic on X and Y sides respectively. Log10Chi2TrackerXInner and Log10Chi2TrackerYInner are the inner tracker track fit Chi2 in logarithmic on X and Y sides respectively. In figure 2, the distributions of these four variables are shown.

3. **Tracker Charge**

Due to the interaction, the tracker charge measurement at the lower part could be contaminated. Therefore, this information could be added to the training variable list. The TrackerL9Charge and TrackerL78Charge are the two variables related to this. TrackerL9Charge is the tracker charge measurement from layer 9. TrackerL78Charge is the mean value of the tracker charge measurement from layer 7 and 8. In figure 3, the distributions of the two variables are shown.

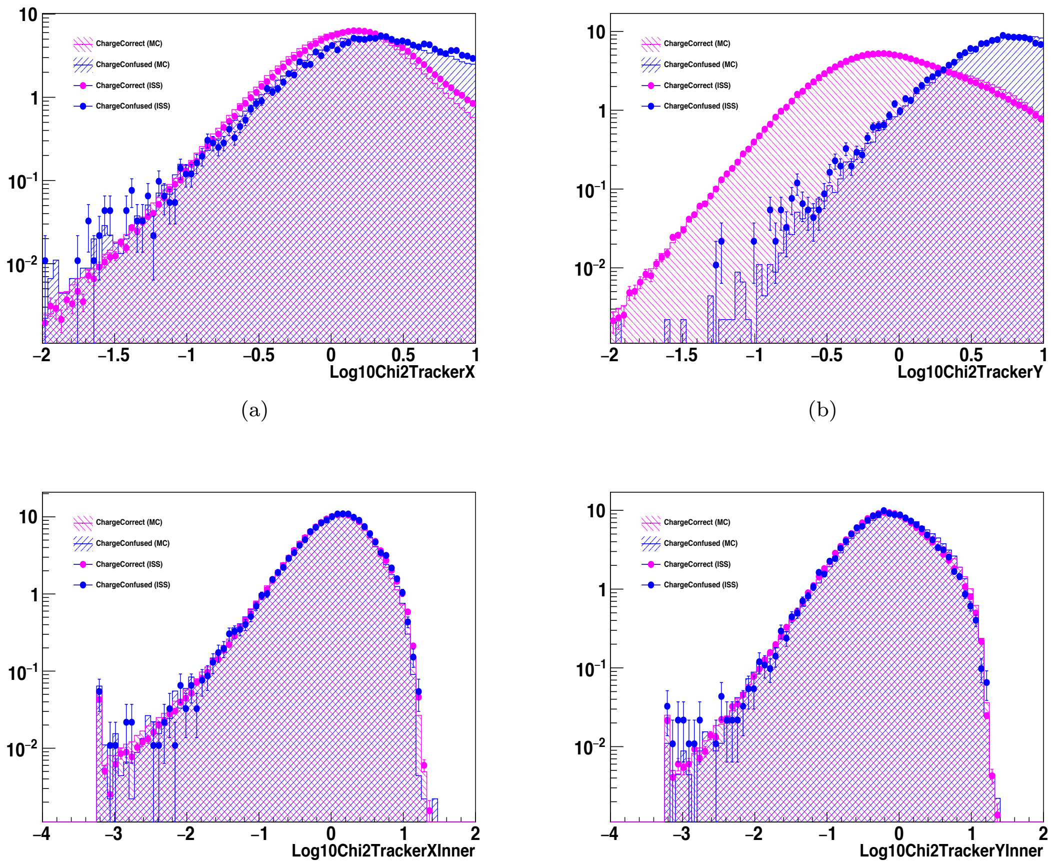


(a) (b) (c) (d)

Figure 2: Distributions of a). Log10Chi2TrackerX b). Log10Chi2TrackerY c). Log10Chi2TrackerXInner d). Log10Chi2TrackerYInner in example rigidity bin of 330 to 525 GV. Histograms (magenta: charge correct; blue: charge confused) are taken from MC and points (magenta: charge correct; blue: charge confused) are from data.

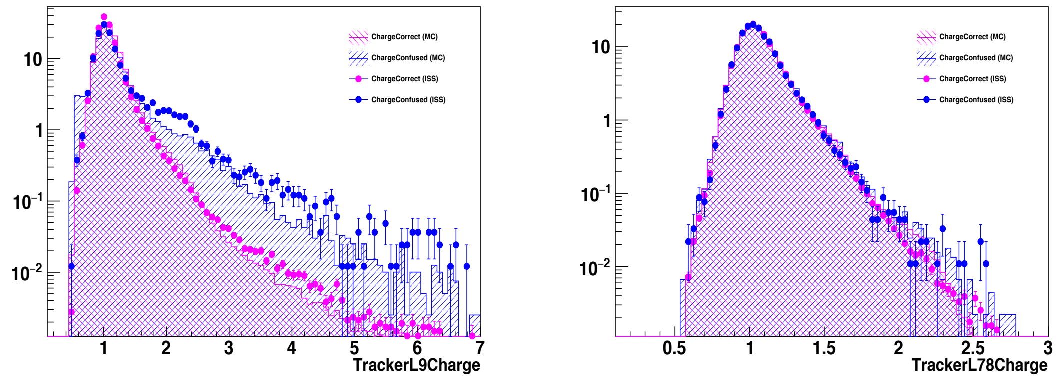


(a) (b)

Figure 3: Distributions of a). TrackerL9Charge b). TrackerL78Charge in example rigidity bin of 330 to 525 GV. Histograms (magenta: charge correct; blue: charge confused) are taken from MC and points (magenta: charge correct; blue: charge confused) are from data.

4. **Charge Asymmetry**

The tracker charge asymmetry also provides information about charge confusion. TrackerL58L24ChargeAsymmetry is the asymmetry of tracker charge measurements and its definition is given below:

$$\text{TrackerL58L24ChargeAsymmetry} = \frac{\text{TrackerL58Charge} - \text{TrackerL24Charge}}{\text{InnerTrackerCharge}}$$

where the TrackerL58Charge is the mean value of the tracker charge from layer 5 and 8. TrackerL24Charge is the mean value of the tracker charge from layer 2 and 4. InnerTrackerCharge is the tracker charge from the inner tracker.

In figure 4, the distributions of the TrackerL58L24ChargeAsymmetry is shown.

5. **TOF Charge**

Except the tracker charge, the charge measurements from the TOF also are used in training. UpperTofCharge and LowerTofCharge are the TOF charge measurements from upper TOF and lower TOF. In figure 5, the distributions of the UpperTofCharge and LowerTofCharge are shown.

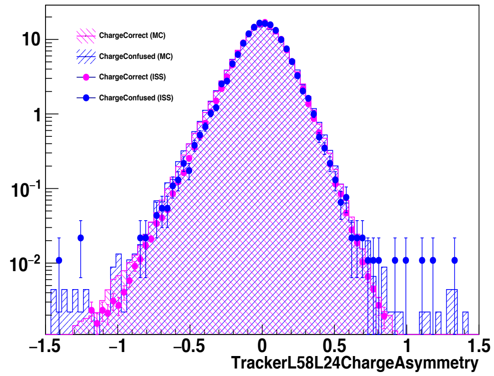


Figure 4: Distributions of TrackerL58L24ChargeAsymmetry in example rigidity bin of 330 to 525 GV. Histograms (magenta: charge correct; blue: charge confused) are taken from MC and points (magenta: charge correct; blue: charge confused) are from data.

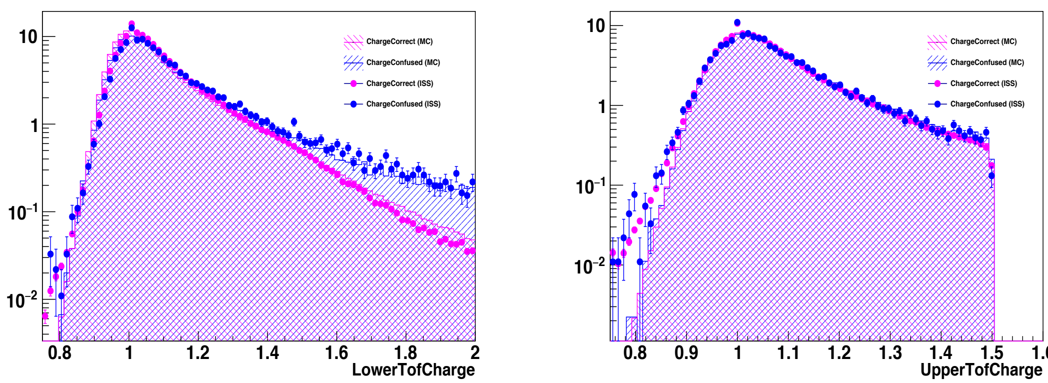


(a) (b)

Figure 5: Distributions of a). LowerTofCharge b). UpperTofCharge in example rigidity bin of 330 to 525 GV. Histograms (magenta: charge correct; blue: charge confused) are taken from MC and points (magenta: charge correct; blue: charge confused) are from data.

6. **TRDLikelihood**

The last variable is the TRDLikelihood. Because of the potential interactions in the TRD for charge confused events, the TRDLikelihood provides the separation power for charge confusion. In figure 6, the distribution of the TRDLikelihood is shown.

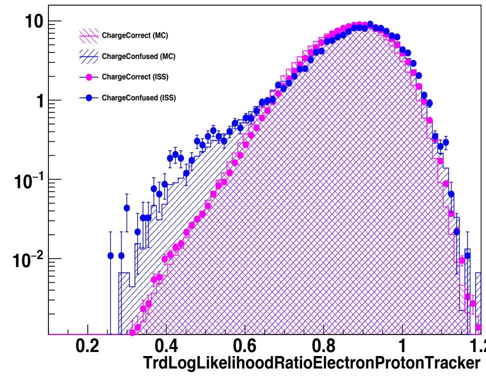


Figure 6: Distributions of TRDLikelihood in example rigidity bin of 330 to 525 GV. Histograms (magenta: charge correct; blue: charge confused) are taken from MC and points (magenta: charge correct; blue: charge confused) are from data.

# APPENDIX

# Acronyms

| | |
|---|---|
| **ACC** | Anti-Coincidence Counters |
| **AMS** | Alpha Magnetic Spectrometer |
| **BDT** | Boosted Decision Tree |
| **CALT** | China Academy of Launch Vehicle Technology |
| **CC** | Charge Confusion |
| **CR** | Cosmic Rays |
| **ECAL** | Electromagnetic Calorimeter |
| **GCR** | Galactic Cosmic Rays |
| **GTB** | Gradient Tree Boosting |
| **HCS** | Heliospheric Current Sheet |
| **HMF** | Heliospheric Magnetic Field |
| **HT** | High Threshold |
| **IGRF** | International Geomagnetic Reference Field |
| **ISM** | Interstellar Medium |
| **ISS** | International Space Station |
| **LEO** | Low Earth Orbit |
| **LIS** | Local Interstellar Spectra |

| | | |
|---|---|---|
| **MHD** | ........................................................... | Magneto-Hydrodynamic |
| **NM** | ........................................................... | Neutron Monitor |
| **PWN** | ........................................................... | Pulsar Wind Nebula |
| **RICH** | ........................................................... | Ring-Imaging Cherenkov detecter |
| **SAA** | ........................................................... | South Atlantic Anomaly |
| **SHT** | ........................................................... | Super High Threshold |
| **SNRs** | ........................................................... | Supernova Remnants |
| **SSN** | ........................................................... | Sunspot Number |
| **SVM** | ........................................................... | Support Vector Machine |
| **TOF** | ........................................................... | Time Of Flight |
| **TOI** | ........................................................... | Top-Of-Instrument |
| **TRD** | ........................................................... | Transition Radiation Detector |
| **TTCS** | ........................................................... | Tracker Thermal Cooling System |

# LIST OF FIGURES

# LIST OF TABLES

# BIBLIOGRAPHY


[1] M. Aguilar et al. (AMS Collaboration). Antiproton Flux, Antiproton-to-Proton Flux Ratio, and Properties of Elementary Particle Fluxes in Primary Cosmic Rays Measured with the Alpha Magnetic Spectrometer on the International Space Station. *Phys. Rev. Lett.*, 117:091103, Aug 2016. DOI: 10.1103/PhysRevLett.117.091103.

[2] NobelPrize.org (Nobel Media AB). Victor F. Hess - Facts, 2022. URL: https://www.nobelprize.org/prizes/physics/1936/hess/facts.

[3] NobelPrize.org (Nobel Media AB). Carl D. Anderson - Facts, 2022. URL: https://www.nobelprize.org/prizes/physics/1936/anderson/facts.

[4] NobelPrize.org (Nobel Media AB). The Nobel Prize in Physics 1959, 2022. URL: https://www.nobelprize.org/prizes/physics/1959/summary.

[5] E. A. Bogomolov, N. D. Lubyanaya, V. A. Romanov, S. V. Stepanov, and M. S. Shulakova. A Stratospheric Magnetic Spectrometer Investigation of the Singly Charged Component Spectra and Composition of the Primary and Secondary Cosmic Radiation. In *International Cosmic Ray Conference*, volume 1, page 330, 1979.

[6] R. L. Golden, S. Horan, B. G. Mauger, G. D. Badhwar, J. L. Lacy, S. A. Stephens, R. R. Daniel, and J. E. Zipse. Evidence for the Existence of Cosmic-Ray Antiprotons. *Phys. Rev. Lett.*, 43:1196–1199, Oct 1979. DOI: 10.1103/PhysRevLett.43.1196.

[7] O. Adriani et al. Measurement of the flux of primary cosmic ray antiprotons with energies of 60-MeV to 350-GeV in the PAMELA experiment. *Pisma Zh. Eksp. Teor. Fiz.*, 96:693–699, 2012. DOI: 10.1134/S002136401222002X.

[8] Kenneth Greisen. End to the Cosmic-Ray Spectrum? *Phys. Rev. Lett.*, 16:748–750, Apr 1966. DOI: 10.1103/PhysRevLett.16.748.

[9] G. T. Zatsepin and V. A. Kuzmin. Upper Limit of the Spectrum of Cosmic Rays. *Soviet Journal of Experimental and Theoretical Physics Letters*, 4:78, Aug 1966. URL: https://www.osti.gov/biblio/4515382.

[10] D. J. Bird et al. Detection of a Cosmic Ray with Measured Energy Well beyond the Expected Spectral Cutoff due to Cosmic Microwave Radiation. *Astrophysical Journal*, 441:144, Mar 1995. DOI: 10.1086/175344.

[11] R. Abbasi et al. Indications of Intermediate-Scale Anisotropy of Cosmic Rays with Energy Greater Than 57 EeV in the Northern Sky Measured with the Surface Detector of the Telescope Array Experiment. *The Astrophysical Journal*, 790(2):L21, Jul 2014. DOI: 10.1088/2041-8205/790/2/l21.

[12] Alicia Lopez Oramas. Multi-year Campaign of the Gamma-Ray Binary LS I $+61^{\circ}$ 303 and Search for VHE Emission from Gamma-Ray Binary Candidates with the MAGIC Telescopes. PhD thesis, Universitat Autonoma de Barcelona, Apr 2015. DOI: 10.13140/RG.2.1.4140.4969.

[13] R. L. et al. (Particle Data Group) Workman. Review of Particle Physics. *PTEP*, 2022:p.083C01, 2022. DOI: 10.1093/ptep/ptac097.

[14] Alessandra Pacini. Cosmic rays: Bringing messages from the sky to the Earth's surface. *Revista Brasileira de Ensino de Fisica*, 39, Jan 2017. DOI: 10.1590/1806-9126-RBEF-2016-0168.

[15] W. Baade and F. Zwicky. Cosmic Rays from Super-novae. *Proceedings of the National Academy of Sciences of the United States of America*, 20(5):259–263, 1934. URL: http://www.jstor.org/stable/86841.

[16] Massimo Turatto. *Classification of* Supernovae, pages 21–36. Springer Berlin Heidelberg, Berlin, Heidelberg, 2003. DOI: 10.1007/3-540-45863-8_3.

[17] Stephen P. Reynolds. Supernova Remnants at High Energy. *Annual Review of Astronomy and Astrophysics*, 46(1):89–126, 2008. DOI: 10.1146/annurev.astro.46.060407.145237.

[18] Malcolm S. Longair. High Energy Astrophysics. UK: Cambridge University Press, 2011. URL: https://ui.adsabs.harvard.edu/abs/2011hea..book.....L.

[19] ENRICO Fermi. On the Origin of the Cosmic Radiation. *Phys. Rev.*, 75:1169–1174, Apr 1949. DOI: 10.1103/PhysRev.75.1169.

[20] T. Gold, F. G. Smith, and A. W. Wolfendale. Pulsars and the Origin of Cosmic Rays and Discussion. *Philosophical Transactions of the Royal Society of London. Series A, Mathematical and Physical Sciences*, 277(1270):453–461, 1975. URL: http://www.jstor.org/stable/74493.

[21] Bednarek, W. and Bartosik, M. Cosmic rays from Galactic pulsars. *Astronomy & Astrophysics*, 423(2):405–413, 2004. DOI: 10.1051/0004-6361:20047005.

[22] J Arons. Pulsar wind nebulae as cosmic pevatrons: A current sheet's tale. *Space Sci Rev*, 173:341–367, 2012. DOI: 10.1007/s11214-012-9885-1.

[23] A. R. Bell. Cosmic ray acceleration in pulsar-driven supernova remnants. *Monthly Notices of the Royal Astronomical Society*, 257(3):493–500, Aug 1992. DOI: 10.1093/mnras/257.3.493.

[24] Dan Hooper, Pasquale Blasi, and Pasquale Dario Serpico. Pulsars as the sources of high energy cosmic ray positrons. *Journal of Cosmology and Astroparticle Physics*, 2009(01):025, Jan 2009. DOI: 10.1088/1475-7516/2009/01/025.

[25] R. Cowsik. Positrons and Antiprotons in Galactic Cosmic Rays. *Annual Review of Nuclear and Particle Science*, 66(1):297–319, 2016. DOI: 10.1146/annurev-nucl-102115-044851.

[26] V Bresci, E Amato, P Blasi, and G Morlino. Effects of re-acceleration and source grammage on secondary cosmic rays spectra. *Monthly Notices of the Royal Astronomical Society*, 488(2):2068–2078, 07 2019. DOI: 10.1093/mnras/stz1806.

[27] Ilias Cholis, Tim Linden, and Dan Hooper. A robust excess in the cosmic-ray antiproton spectrum: Implications for annihilating dark matter. *Phys. Rev. D*, 99:103026, May 2019. DOI: 10.1103/PhysRevD.99.103026.

[28] Jan Heisig. Cosmic-ray antiprotons in the ams-02 era: A sensitive probe of dark matter. *Modern Physics Letters A*, 36(05):2130003, 2021. DOI: 10.1142/S0217732321300032.

[29] Martin Wolfgang Winkler. Cosmic ray antiprotons at high energies. *Journal of Cosmology and*

*Astroparticle Physics*, 2017(02):048–048, Feb 2017. DOI: 10.1088/1475-7516/2017/02/048.

[30] Rolf Kappl and Martin Wolfgang Winkler. The cosmic ray antiproton background for AMS-02. *Journal of Cosmology and Astroparticle Physics*, 2014(09):051–051, Sep 2014. DOI: 10.1088/1475-7516/2014/09/051.

[31] Ming-Yang Cui, Qiang Yuan, Yue-Lin Sming Tsai, and Yi-Zhong Fan. Possible dark matter annihilation signal in the ams-02 antiproton data. *Phys. Rev. Lett.*, 118:191101, May 2017. DOI: 10.1103/PhysRevLett.118.191101.

[32] Andrew W. Strong, Igor V. Moskalenko, and Vladimir S. Ptuskin. Cosmic-Ray Propagation and Interactions in the Galaxy. *Annual Review of Nuclear and Particle Science*, 57(1):285–327, 2007. DOI: 10.1146/annurev.nucl.57.090506.123011.

[33] Igor V. Moskalenko. Galprop: modeling cosmic ray propagation and associated interstellar emissions, 2011. DOI: 10.48550/ARXIV.1105.4921.

[34] David Maurin. usine: Semi-analytical models for Galactic cosmic-ray propagation. *Computer Physics Communications*, 247:106942, 2020. DOI: 10.1016/j.cpc.2019.106942.

[35] Carmelo Evoli, Daniele Gaggero, Andrea Vittino, Giuseppe Di Bernardo, Mattia Di Mauro, Arianna Ligorini, Piero Ullio, and Dario Grasso. Cosmic-ray propagation with DRAGON2: I. numerical solver and astrophysical ingredients. *Journal of Cosmology and Astroparticle Physics*, 2017(02):015–015, Feb 2017. DOI: 10.1088/1475-7516/2017/02/015.

[36] V. S. Ptuskin, O. N. Strelnikova, and L. G. Sveshnikova. On leaky-box approximation to GALPROP. *Astropart. Phys.*, 31:284–289, 2009. DOI: 10.1016/j.astropartphys.2009.02.004.

[37] E. N. Parker. Dynamics of the Interplanetary Gas and Magnetic Fields. *Astrophysical Journal*, 128:664, Nov 1958. DOI: 10.1086/146579.

[38] Christopher T. Russell. The Solar Wind and Magnetospheric Dynamics. In *Correlated Interplanetary and Magnetospheric Observations*, pages 3–47, Dordrecht, 1974. Springer Netherlands. DOI: 10.1007/978-94-010-2172-2_1.

[39] M.J. Owens and R.J. Forsyth. The Heliospheric Magnetic Field. *Living Rev. Sol. Phys.*, 10, Nov 2013. DOI: 10.12942/lrsp-2013-5.

[40] A. J. Dessler. Solar wind and interplanetary magnetic field. *Reviews of Geophysics*, 5(1):1–41, 1967. DOI: 10.1029/RG005i001p00001.

[41] R Cowen. Voyager 1 has reached interstellar space. *Nature*, 2013. DOI: 10.1038/nature.2013.13735.

[42] NASA. Solar wind at voyager 1, 2012. Retrieved 16:20, July 20, 2022 from: https://commons.wikimedia.org/wiki/File:Solar_wind_at_Voyager_1.png.

[43] David H. Hathaway. The Solar Cycle. *Living Reviews in Solar Physics*, 7(1):1, Dec 2010. DOI: 10.12942/lrsp-2010-1.

[44] Carsten Jorgensen, Christoffer Karoff, Senthamizh Pavai Valliappan, and Rainer Arlt. Chris-

tian Horrebow's Sunspot Observations – I. Life and Published Writings. *Solar Physics*, Jun 2019. DOI: 10.1007/s11207-019-1465-z.

[45] Christoffer Karoff, Carsten Jorgensen, Senthamizh Pavai Valliappan, and Rainer Arlt. Christian Horrebow's Sunspot Observations – II. Construction of a Record of Sunspot Positions. *Solar Physics*, 294, Jun 2019. DOI: 10.1007/s11207-019-1466-y.

[46] Gleeson.L and Axford.W. Solar Modulation of Galactic Cosmic Rays. *Astrophysical Journal*, 154:1011, Dec 1968. DOI: 10.1086/149822.

[47] Eddie Ross and William J. Chaplin. The behaviour of galactic cosmic ray intensity during solar activity cycle 24. *Solar Physics*, 294(1):8, Jan 2019. DOI: 10.1007/s11207-019-1397-7.

[48] M. Aguilar et al. (AMS Collaboration). Observation of complex time structures in the cosmic-ray electron and positron fluxes with the alpha magnetic spectrometer on the international space station. *Phys. Rev. Lett.*, 121:051102, Jul 2018. DOI: 10.1103/PhysRevLett.121.051102.

[49] K. Anraku et al. Balloon borne experiment using a superconducting solenoidal magnet spectrometer. In *KEK-PREPRINT-94-40*, 6 1994. URL: https://lib-extopc.kek.jp/preprints/PDF/1994/9427/9427040.pdf.

[50] M. Nozaki. BESS-Polar. *Nuclear Instruments and Methods in Physics Research Section B: Beam Interactions with Materials and Atoms*, 214:110–115, 2004. DOI: 10.1016/j.nimb.2003.08.005.

[51] T. Yoshida, A. Yamamoto, and J. et al. Mitchell. Bess-polar experiment. *Life sciences and space research*, 33(10):1755–1762, 2004. DOI: 10.1016/j.asr.2003.05.017.

[52] K. Abe et al. Measurement of the cosmic-ray low-energy antiproton spectrum with the first BESS-Polar Antarctic flight. *Physics Letters B*, 670(2):103–108, 2008. DOI: 10.1016/j.physletb.2008.10.053.

[53] K. Abe et al. Measurement of the Cosmic-Ray Antiproton Spectrum at Solar Minimum with a Long-Duration Balloon Flight over Antarctica. *Phys. Rev. Lett.*, 108:051102, Jan 2012. DOI: 10.1103/PhysRevLett.108.051102.

[54] A M Galper et al. The PAMELA experiment: a decade of Cosmic Ray Physics in space. *Journal of Physics: Conference Series*, 798:012033, Jan 2017. DOI: 10.1088/1742-6596/798/1/012033.

[55] O. Adriani et al. (PAMELA Collaboration). New Measurement of the Antiproton-to-Proton Flux Ratio up to 100 GeV in the Cosmic Radiation. *Phys. Rev. Lett.*, 102:051101, Feb 2009. DOI: 10.1103/PhysRevLett.102.051101.

[56] O. Adriani et al. (PAMELA Collaboration). PAMELA Results on the Cosmic-Ray Antiproton Flux from 60 MeV to 180 GeV in Kinetic Energy. *Phys. Rev. Lett.*, 105:121101, Sep 2010. DOI: 10.1103/PhysRevLett.105.121101.

[57] S. et al. Ahlen. An antimatter spectrometer in space. *Nuclear Instruments and Methods in Physics Research Section A: Accelerators, Spectrometers, Detectors and Associated Equipment*, 350(1):351–367, 1994. DOI: 10.1016/0168-9002(94)91184-3.

[58] Roberto Battiston. The antimatter spectrometer (AMS-02): A particle physics detector in space. *Nuclear Instruments and Methods in Physics Research Section A: Accelerators, Spectrometers, Detectors and Associated Equipment*, 588(1):227–234, 2008. DOI: 10.1016/j.nima.2008.01.044.

[59] M Aguilar et al. The Alpha Magnetic Spectrometer (AMS) on the International Space Station: Part I - results from the test flight on the space shuttle. *Physics Reports*, 366(6):331–405, 2002. DOI: 10.1016/S0370-1573(02)00013-3.

[60] Roskosmos. STS-91 PLB, 1998. Retrieved 16:20, July 20, 2022 from: https://commons.wikimedia.org/wiki/File:STS-91_PLB.jpg.

[61] NASA/Crew-2. View of the ISS taken during crew-2 flyaround (iss066-e-081311), 2021. Retrieved 16:20, July 20, 2022 from: https://commons.wikimedia.org/wiki/File:View_of_the_ISS_taken_during_Crew-2_flyaround_(ISS066-E-081311).jpg.

[62] Zoe Budrikis. A decade of AMS-02. *Nature Reviews Physics*, 3(5):308–308, Jan 2021. DOI: 10.1038/s42254-021-00320-7.

[63] Fabian Machate. *Study for large acceptance electron analysis with the Alpha Magnetic Spectrometer on the International Space Station*. Dissertation, RWTH Aachen University, Aachen, 2021. DOI: 10.18154/RWTH-2021-09976.

[64] AMS Collaboration. The Alpha Magnetic Spectrometer on the International Space Station, 2022. URL: https://ams02.space.

[65] V. L. Ginzburg and I. M. Frank. Radiation of a uniformly moving electron due to its transition from one medium into another. *J. Phys. (USSR)*, 9:353–362, 1945.

[66] M. Heil et al. Operations and Alignment of the AMS-02 Transition Radiation Detector. In *33rd International Cosmic Ray Conference*, page 1232, 2013. URL: https://galprop.stanford.edu/elibrary/icrc/2013/papers/icrc2013-1232.pdf.

[67] T. Siedenburg. The AMS TRD. A gasdetector designed for operation in space. *Nuclear Physics B - Proceedings Supplements*, 150:30–33, 2006. DOI: 10.1016/j.nuclphysbps.2004.06.001.

[68] Thomas Kirn. The AMS-02 TRD on the international space station. *Nuclear Instruments and Methods in Physics Research Section A: Accelerators, Spectrometers, Detectors and Associated Equipment*, 706:43–47, 2013. DOI: 10.1016/j.nima.2012.05.010.

[69] Jerzy Neyman, Egon Sharpe Pearson, and Karl Pearson. Ix. On the problem of the most efficient tests of statistical hypotheses. *Philosophical Transactions of the Royal Society of London. Series A, Containing Papers of a Mathematical or Physical Character*, 231(694-706):289–337, 1933. DOI: 10.1098/rsta.1933.0009.

[70] B. Blau, S.M. Harrison, H. Hofer, S.R. Milward, J.S.H. Ross, S.C.C. Ting, J. Ulbricht, and G. Viertel. The superconducting magnet of ams-02. *Nuclear Physics B - Proceedings Supplements*, 113(1):125–132, 2002. DOI: 10.1016/S0920-5632(02)01831-5.

[71] K. Lubelsmeyer et al. Upgrade of the Alpha Magnetic Spectrometer (AMS-02) for long term

operation on the International Space Station (ISS). *Nuclear Instruments and Methods in Physics Research Section A: Accelerators, Spectrometers, Detectors and Associated Equipment*, 654(1):639–648, 2011. DOI: 10.1016/j.nima.2011.06.051.

[72] Pierre Erwan Saouter. Operation and Performance of AMS-02 Silicon Tracker. *PoS*, Vertex2014:028, 2015. DOI: 10.22323/1.227.0028.

[73] Sadakazu Haino. Performance of the AMS-02 silicon tracker in the ISS mission. *Nucl. Instrum. Meth. A*, 699:221–224, 2013. DOI: 10.1016/j.nima.2012.05.060.

[74] G. Ambrosi et al. Alignment of the AMS-02 Silicon Tracker. In *33rd International Cosmic Ray Conference*, page 1260, 2013. URL: https://ui.adsabs.harvard.edu/abs/2013ICRC...33..570A.

[75] B. Alpat et al. The internal alignment and position resolution of the ams-02 silicon tracker determined with cosmic-ray muons. *Nuclear Instruments and Methods in Physics Research Section A: Accelerators, Spectrometers, Detectors and Associated Equipment*, 613(2):207–217, 2010. DOI: 10.1016/j.nima.2009.11.065.

[76] V. Bindi et al. Calibration and performance of the AMS-02 time of flight detector in space. *Nucl. Instrum. Meth. A*, 743:22–29, 2014. DOI: 10.1016/j.nima.2014.01.002.

[77] V. Bindi, A. Contin, N. Masi, A. Oliva, F. Palmonari, L. Quadrani, and A. Tiseni. The time of flight detector of the AMS-02 experiment on the international space station. *Nucl. Instrum. Meth. A*, 718:478–480, 2013. DOI: 10.1016/j.nima.2012.11.061.

[78] V. Bindi, E. Choumilov, A. Contin, N. Masi, A. Oliva, F. Palmonari, L. Quadrani, and Q. Yan. The AMS-02 Time of Flight (TOF) System: Construction and Overall Performances in Space. In *International Cosmic Ray Conference*, volume 33 of *International Cosmic Ray Conference*, page 2298, Jan 2013. URL: https://ui.adsabs.harvard.edu/abs/2013ICRC...33.2298B.

[79] Hu Liu, J. Casaus, F. Giovacchini, A. Oliva, and X. Xia. The RICH detector of AMS-02: 5 years of operation in space. *Nucl. Instrum. Meth. A*, 876:5–8, 2017. DOI: 10.1016/j.nima.2016.12.011.

[80] R. Pereira. The AMS-02 RICH detector: Performance during ground-based data taking at CERN. *Nucl. Instrum. Meth. A*, 639:37–41, 2011. DOI: 10.1016/j.nima.2010.09.036.

[81] F. Giovacchini, J. Casaus, and A. Oliva. The AMS-02 RICH detector: Status and physics results. *Nuclear Instruments and Methods in Physics Research Section A: Accelerators, Spectrometers, Detectors and Associated Equipment*, 952:161797, 2020. DOI: 10.1016/j.nima.2019.01.024.

[82] F. Giovacchini. Performance in space of the AMS-02 RICH detector. *Nuclear Instruments and Methods in Physics Research Section A: Accelerators, Spectrometers, Detectors and Associated Equipment*, 766:57–60, 2014. DOI: 10.1016/j.nima.2014.04.036.

[83] Sylvie Rosier-Lees. Performance of the AMS02 electromagnetic calorimeter in space. *J. Phys. Conf. Ser.*, 404:012034, 2012. DOI: 10.1088/1742-6596/404/1/012034.

[84] M. Vecchi et al. The electromagnetic calorimeter of the AMS-02 experiment. In *Semaine de l'Astrophysique Francaise (SF2A 2012)*, Nice, France, Jun 2012. URL: http://hal.in2p3.fr/in2p3-00745677.

[85] C. Adloff et al. The AMS-02 lead-scintillating fibres Electromagnetic Calorimeter. *Nucl. Instrum. Meth. A*, 714:147–154, 2013. DOI: 10.1016/j.nima.2013.02.020.

[86] Marco Incagli. Performance of the AMS-02 Electromagnetic Calorimeter in Space. *PoS*, TIPP2014:025, 2014. DOI: 10.22323/1.213.0025.

[87] Manuela Vecchi, Kaiyuan Wu, and Yuan-Hann Chang. A 3-dimensional electromagnetic shower characterization and its application to AMS-02 pointing capability. In *33rd International Cosmic Ray Conference*, page 0653, 2013.

[88] Stefano Di Falco. Results of 2007 test beam of AMS-02 Electromagnetic Calorimeter. *Adv. Space Res.*, 45:112–122, 2010. DOI: 10.1016/j.asr.2009.08.005.

[89] G Gallucci and (for the AMS-02 ECAL group). Performance of the AMS-02 Electromagnetic Calorimeter in Space. *Journal of Physics: Conference Series*, 587:012028, Feb 2015. DOI: 10.1088/1742-6596/587/1/012028.

[90] Ph. von Doetinchem, W. Karpinski, Th. Kirn, K. Luebelsmeyer, St. Schael, and M. Wlochal. The AMS-02 Anticoincidence Counter. *Nucl. Phys. B Proc. Suppl.*, 197:15–18, 2009. DOI: 10.1016/j.nuclphysbps.2009.10.025.

[91] T. Bruch and W. Wallraff. The Anti-Coincidence Counter shield of the AMS tracker. *Nucl. Instrum. Meth. A*, 572:505–507, 2007. DOI: 10.1016/j.nima.2006.10.376.

[92] A. Basili, V. Bindi, D. Casadei, G. Castellini, A. Contin, A. Kounine, M. Lolli, F. Palmonari, and L. Quadrani. The TOF-ACC flight electronics for the fast trigger and time of flight of the AMS-02 cosmic ray spectrometer. *Nucl. Instrum. Meth. A*, 707:99–113, 2013. DOI: 10.1016/j.nima.2012.12.089.

[93] Ph. von Doetinchem, Th. Kirn, K. Luebelsmeyer, and St. Schael. The Anticoincidence Counter System of AMS-02, 2009. DOI: 10.48550/ARXIV.0906.1068.

[94] Rene Brun and Fons Rademakers. Root - An object oriented data analysis framework. *Nuclear Instruments and Methods in Physics Research Section A: Accelerators, Spectrometers, Detectors and Associated Equipment*, 389(1):81–86, 1997. DOI: 10.1016/S0168-9002(97)00048-X.

[95] Bastian Beischer. *Measurement of high energy gamma rays from 200 MeV to 1 TeV with the Alpha Magnetic Spectrometer on the International Space Station*. Dissertation, RWTH Aachen University, Aachen, 2020. DOI: 10.18154/RWTH-2020-06535.

[96] M. Aguilar et al. (AMS Collaboration). Precision Measurement of the Proton Flux in Primary Cosmic Rays from Rigidity 1 GV to 1.8 TV with the Alpha Magnetic Spectrometer on the International Space Station. *Phys. Rev. Lett.*, 114:171103, Apr 2015. DOI: 10.1103/PhysRevLett.114.171103.

[97] J. Bartels. Twenty-seven day recurrences in terrestrial-magnetic and solar activity, 1923-1933. *Terrestrial Magnetism and Atmospheric Electricity*, 39(3):201–202a, 1934. DOI: 10.1029/TE039i003p00201.

[98] S. Agostinelli et al. GEANT4–a simulation toolkit. *Nucl. Instrum. Meth. A*, 506:250–303, 2003. DOI: 10.1016/S0168-9002(03)01368-8.

[99] J. Allison et al. Recent developments in Geant4. *Nucl. Instrum. Meth. A*, 835:186–225, 2016. DOI: 10.1016/j.nima.2016.06.125.

[100] Paolo Zuccon. AMS-02 Track reconstruction and rigidity measurement. In *33rd International Cosmic Ray Conference*, page 1064, 2013. URL: https://s3.cern.ch/inspire-prod-files-7/71c48c76263c1f7bee2621c779ba3320.

[101] Helge Voss, Andreas Hocker, Jorg Stelzer, and Fredrik Tegenfeldt. TMVA, the toolkit for multivariate data analysis with ROOT. In XI International Workshop on Advanced Computing and Analysis Techniques in Physics Research, volume 50, page 040. SISSA Medialab, 2009. DOI: 10.22323/1.050.0040.

[102] J.D. Sullivan. Geometric factor and directional response of single and multi-element particle telescopes. *Nuclear Instruments and Methods*, 95(1):5–11, 1971. DOI: 10.1016/0029-554X(71)90033-4.

[103] Nikolas Zimmermann. *Precision measurement of the cosmic-ray electron and positron fluxes as a function of time and energy with the Alpha Magnetic Spectrometer on the International Space Station*. Dissertatison, RWTH Aachen University, Aachen, 2020. DOI: 10.18154/RWTH-2020-02650.

[104] Carl Stormer. The polar aurora. *Quarterly Journal of the Royal Meteorological Society*, 82(351):115–115, 1956. DOI: 10.1002/qj.49708235123.

[105] G. D'Agostini. A multidimensional unfolding method based on Bayes' theorem. *Nuclear Instruments and Methods in Physics Research Section A: Accelerators, Spectrometers, Detectors and Associated Equipment*, 362(2):487–498, 1995. DOI: 10.1016/0168-9002(95)00274-X.

[106] Tim Adye. Unfolding algorithms and tests using RooUnfold. In *PHYSTAT 2011*, pages 313–318, Geneva, 2011. CERN. DOI: 10.5170/CERN-2011-006.313.

[107] M. Aguilar et al. (AMS Collaboration). The Alpha Magnetic Spectrometer (AMS) on the international space station: Part II – Results from the first seven years. *Physics Reports*, 894:1–116, 2021. DOI: 10.1016/j.physrep.2020.09.003.

[108] Marius S. Potgieter, O. P. M. Aslam, Driaan Bisschoff, and Donald Ngobeni. A perspective on the solar modulation of cosmic anti-matter. *Physics*, 3(4):1190–1225, 2021. DOI: 10.3390/physics3040076.

[109] John W. Bieber, R. A. Burger, Ralph Engel, Thomas K. Gaisser, Stefan Roesler, and Todor Stanev. Antiprotons at solar maximum. *Phys. Rev. Lett.*, 83:674–677, Jul 1999. DOI: 10.1103/PhysRevLett.83.674.

[110] S. Schael et al. AMS-100: The next generation magnetic spectrometer in space - An international science platform for physics and astrophysics at Lagrange point 2. *Nuclear Instruments and Methods in Physics Research Section A: Accelerators, Spectrometers, Detectors and Associated Equipment*, 944:162561, 2019. DOI: 10.1016/j.nima.2019.162561.

# Acknowledgements

First, I would like to thank Prof. Dr. Stefan Schael to give me the opportunity to work in his institute and also as a member of the AMS-02 collaboration. During the last few years, I can always benefit from his supervision and guidance. His passion for Physics and enthusiasm really inspire me. Also, I learn a lot from his ambitions to push things forward.

I would also like to thank Prof. Dr. Christopher Wiebusch for agreeing to be my second supervisor for the thesis.

Second, I would also like to thank Prof. Samuel Ting, the PI of the whole AMS-02 experiment. Without his effort in the last decades, the AMS-02 project would not come true. His spirit of never giving up will inspire me in the future. In addition, I admire his concentration and perseverance shown in his career.

Many friends and colleagues helped me a lot during my PhD time in Aachen. Special thanks to Robin Sonnabend who helped me from zero ground when I was a beginner in AMS. He is always patient to teach me and answer stupid questions. I would like to thank Dr. Henning Gast. As the actual host in the Aachen analysis group, he put a lot of effort to support the Aachen data analysis.

During my PhD study in the institute, many friends and colleagues make my working time pleasant: Dr. Nikolas Zimmermann, Dr. Bastian Beischer, Dr. Fabian Machate, Dr. Nikolay Nikonov, Dr. Leila Ali Cavasonza, Dr. Sofia Chouridou, Manbing Li, Emiliano Rampi, Yasaman Najafi. I can always learn a lot from discussions with you, and the time I spent with you guys has already been a precious memory for me.

I would like to thank again to Dr. Henning Gast and Dr. Sofia Chouridou who did proofreadings for this thesis. Many thanks for your time and valuable comments.

I would like to thank Georg Schwering, Natalie Driessen, Tanja Bingler and Gina Wilden for their support work in the administration branch of the institute. As a foreigner working in Aachen, i was guided by them in almost every step of my PhD program.

During my shift at CERN, many friends and colleagues there make my stay enjoyable. I would like to thank Dr. Mike Capell, Dr. Zhili Weng, Dr. Weiwei Xu, Dr. Valery Zhukov, Dr. Youmin Yu, Dr. Baosong Shan, Dr. Yi Jia, Dr. XiaoTing Qin, and so many people. The talks at POCC can always make the time delightful.

Last but foremost, I would like to thank my family. The forever love and encouragement are the sources of power for me that support me all the time. The thesis wouldn't be done without your sacrifice behind.